Author(s): Tuovinen, Toni & Hinkkanen, Marko

Title: Signal-injection assisted full-order observer with parameter adaptation for synchronous reluctance motor drives

Year: 2013

Version: Post print

Please cite the original version:

Tuovinen, Toni & Hinkkanen, Marko. 2013. Signal-injection assisted full-order observer with parameter adaptation for synchronous reluctance motor drives. 2013 IEEE Energy Conversion Congress and Exposition (ECCE). 8. DOI: 10.1109/ecce.2013.6647160.

Signal-Injection Assisted Full-Order Observer with Parameter Adaptation for Synchronous Reluctance Motor Drives

Toni Tuovinen and Marko Hinkkanen

Aalto University School of Electrical Engineering
P.O. Box 13000, FI-00076 Aalto, Finland

***Abstract*—A back-EMF-based position observer for motion-sensorless synchronous reluctance motor (SyRM) drives is augmented with parameter-adaptation laws for improved low, medium, and high speed operation. The augmented observer is experimentally evaluated using a 6.7-kW SyRM drive under various speeds and load conditions. The analysis and experimental results indicate that the stator-resistance adaptation should be enabled only at low speeds, the d-axis inductance adaptation should be enabled only at medium and high speeds near no load, and the q-axis inductance adaptation should be enabled only at high speeds under high load.**

***Index Terms*—Inductance adaptation, observer, parameter adaptation, parameter uncertainties, resistance adaptation, signal-injection, speed sensorless, stability conditions.**

I. Introduction

The synchronous reluctance motor (SyRM) has recently reemerged as a contender to the induction motor in variable-speed drives [1]–[3]. As compared to the permanent-magnet synchronous motor (PMSM), the SyRM is magnetized from the stator winding, which renders field-weakening operation a straightforward procedure. The fluctuating price of rare-earth metals has also made the SyRM more favorable in relation to the PMSM.

In order to operate synchronous machines, the position of the rotor has to be either measured or estimated. Position-sensorless operation is commonly preferred. At high speeds, methods based on the back electromotive force (EMF) can be used. Since the SyRM can be seen as a special case of the salient PMSM, back-EMF-based methods suitable for salient PMSMs can be used for SyRMs with slight modifications.

The back-EMF-based methods fail to estimate the position at low speeds and standstill. As the SyRM is inherently salient, methods providing a rotor-position estimate even at standstill are readily applicable. These methods can be roughly categorized as

- signal-injection methods [1], [3]–[6]
- modified PWM [7], [8]
- methods based on stator current variation without additional signal [9], [10].

Since the signal-injection methods inflict additional noise and losses, back-EMF-based position estimation methods are a desirable starting point. The underlying back-EMF-based observer is augmented with additional information from a signal-injection based method only at the lowest speeds [1], [11]–[13].

In this paper, an adaptive full-order observer is augmented with parameter-adaptation laws for a SyRM drive in order to improve low, medium, and high-speed operation. SyRMs are usually magnetically saturated in the rated operating point. The d-axis flux component saturates strongly as a function of the corresponding current component, and the d-axis saturation is coupled with the q-axis saturation. For improved medium and high-speed operation, the inductance estimates are adjusted using a back-EMF-based method. The proposed inductance-adaptation method can be used to obtain saturation-model parameters in an initialization test in a fashion similar to [14], after which the saturation-model parameters are locked.

The stator resistance depends on the temperature. At low speeds, the stator-resistance estimate is adjusted using a high-frequency signal-injection method. The method proposed in this paper is of lower order than the method proposed in [15], where the information provided by the signal-injection method was used via introducing a fictitious speed-correction parameter, which was then utilized to update the resistance estimate. Since the signal injection affects the dynamics of the underlying back-EMF-based observer, additional focus should be put on the tuning of the augmented observer. Reduction of the complexity of the observer simplifies the analysis and the tuning procedure.

After a review of the motor model in Section II, and the rotor-position observer in Section III, the main contributions of the paper are presented Sections IV and V:

1) Adaptation law to adjust the inductance estimates at medium and high speeds using a back-EMF-based method is proposed.
2) Analytical equations for steady-state position- and inductance-estimation errors are derived, taking into account errors in the other parameter estimates.
3) Adaptation law to adjust the stator-resistance estimate at low speeds using a signal-injection based method is proposed.
4) Analytical equation for steady-state resistance-estimation error is derived, and a stabilizing gain

selection is proposed, based on the analytical stability conditions.

The experimental setup is described in Section VI, and the performance of the proposed observer design is evaluated using laboratory experiments with a 6.7-kW SyRM drive in Section VII.

II. SyRM Model

Real space vectors will be used here. For example, the stator-current vector is $\boldsymbol{i}_\mathrm{s} = [i_\mathrm{d}, i_\mathrm{q}]^\mathrm{T}$, where i_d and i_q are the components of the vector and the matrix transpose is marked with the superscript T. The orthogonal rotation matrix is defined as

$$\mathbf{J} = \begin{bmatrix} 0 & -1 \\ 1 & 0 \end{bmatrix}.$$

The electrical position of the d-axis is denoted by ϑ_m. The d-axis is defined as the direction of the maximum inductance of the rotor. The position depends on the electrical angular rotor speed ω_m according to

$$\frac{\mathrm{d}\vartheta_\mathrm{m}}{\mathrm{d}t} = \omega_\mathrm{m} \tag{1a}$$

To simplify the analysis in the following sections, the machine model will be expressed in the *estimated* rotor reference frame, whose d-axis is aligned at $\hat{\vartheta}_\mathrm{m}$ with respect to the stator reference frame. The stator inductance is

$$\boldsymbol{L} = \mathrm{e}^{-\tilde{\vartheta}_\mathrm{m}\mathbf{J}} \begin{bmatrix} L_\mathrm{d} & 0 \\ 0 & L_\mathrm{q} \end{bmatrix} \mathrm{e}^{\tilde{\vartheta}_\mathrm{m}\mathbf{J}} \tag{1b}$$

where $\tilde{\vartheta}_\mathrm{m} = \hat{\vartheta}_\mathrm{m} - \vartheta_\mathrm{m}$ is the estimation error in the rotor position, L_d the direct-axis inductance, and L_q the quadrature-axis inductance. The voltage equation is

$$\frac{\mathrm{d}\boldsymbol{\psi}_\mathrm{s}}{\mathrm{d}t} = \boldsymbol{u}_\mathrm{s} - R_\mathrm{s}\boldsymbol{i}_\mathrm{s} - \hat{\omega}_\mathrm{m}\mathbf{J}\boldsymbol{\psi}_\mathrm{s} \tag{1c}$$

where $\boldsymbol{\psi}_\mathrm{s}$ is the stator-flux vector, $\boldsymbol{u}_\mathrm{s}$ the stator-voltage vector, R_s the stator resistance, and $\hat{\omega}_\mathrm{m} = \mathrm{d}\hat{\vartheta}_\mathrm{m}/\mathrm{d}t$ is the angular speed of the coordinate system. The stator current is a non-linear function

$$\boldsymbol{i}_\mathrm{s} = \boldsymbol{L}^{-1}\boldsymbol{\psi}_\mathrm{s} \tag{1d}$$

of the stator-flux vector and the position error $\tilde{\vartheta}_\mathrm{m}$.

III. Adaptive Full-Order Observer

In the adaptive full-order observer [15], [16], the stator-flux vector is estimated according to

$$\frac{\mathrm{d}\hat{\boldsymbol{\psi}}_\mathrm{s}}{\mathrm{d}t} = \boldsymbol{u}_\mathrm{s} - \hat{R}_\mathrm{s}\hat{\boldsymbol{i}}_\mathrm{s} - \hat{\omega}_\mathrm{m}\mathbf{J}\hat{\boldsymbol{\psi}}_\mathrm{s} + \boldsymbol{K}\tilde{\boldsymbol{i}}_\mathrm{s}, \quad \hat{\boldsymbol{i}}_\mathrm{s} = \hat{\boldsymbol{L}}^{-1}\hat{\boldsymbol{\psi}}_\mathrm{s} \tag{2}$$

where $\hat{\boldsymbol{i}}_\mathrm{s}$ is the estimated stator-current vector, $\tilde{\boldsymbol{i}}_\mathrm{s} = \hat{\boldsymbol{i}}_\mathrm{s} - \boldsymbol{i}_\mathrm{s}$ is the estimation error of the stator current, $\boldsymbol{K}$ is the gain matrix, and $\hat{R}_\mathrm{s}$ is the estimated stator resistance. The gain matrix is [17]

$$\boldsymbol{K} = \begin{bmatrix} \hat{R}_\mathrm{s} + \hat{L}_\mathrm{d}k_1 & -\hat{L}_\mathrm{q}\beta k_1 \\ \hat{L}_\mathrm{d}k_2 & \hat{R}_\mathrm{s} - \hat{L}_\mathrm{q}\beta k_2 \end{bmatrix} \tag{3a}$$

where $\hat{L}_\mathrm{d}$ and $\hat{L}_\mathrm{q}$ are the estimated d and q axis inductances, respectively, $\beta = i_\mathrm{q}/i_\mathrm{d}$, and k_1 and k_2 are given by

$$k_1 = -\frac{b + \beta(c/\hat{\omega}_\mathrm{m} - \hat{\omega}_\mathrm{m})}{\beta^2 + 1}, \quad k_2 = \frac{\beta b - c/\hat{\omega}_\mathrm{m} + \hat{\omega}_\mathrm{m}}{\beta^2 + 1} \tag{3b}$$

where the design parameters b and c should be positive.

The rotor speed is estimated with the PI mechanism

$$\hat{\omega}_\mathrm{m} = \boldsymbol{k}_\mathrm{p}\tilde{\boldsymbol{i}}_\mathrm{s} + \int \boldsymbol{k}_\mathrm{i}\tilde{\boldsymbol{i}}_\mathrm{s}\mathrm{d}t \tag{4}$$

The gain vectors $\boldsymbol{k}_\mathrm{p} = [0, k_\mathrm{p}]$ and $\boldsymbol{k}_\mathrm{i} = [0, k_\mathrm{i}]$ are chosen to utilize the estimation error only in the q axis direction. For convenience, the gains k_p and k_i are selected according to

$$k_\mathrm{p} = \frac{\hat{L}_\mathrm{q}d}{(\hat{L}_\mathrm{d} - \hat{L}_\mathrm{q})i_\mathrm{d}}, \quad k_\mathrm{i} = \frac{\hat{L}_\mathrm{q}e}{(\hat{L}_\mathrm{d} - \hat{L}_\mathrm{q})i_\mathrm{d}} \tag{5}$$

where d and e are design parameters, which may depend on the rotor speed. With this gain selection, the characteristic polynomial of the closed-loop system consisting of (1) – (5) can, after linearization, be split into a product of two second-order polynomials,

$$(s^2 + bs + c)(s^2 + ds + e) \tag{6}$$

and the stability is guaranteed for all positive values of b, c, d, and e, if the parameter estimates are accurate. The observer is of the fourth order, and there are four gains. In order to reduce the number of design parameters, d and e can be chosen as [18]

$$d = 2\rho, \quad e = \rho^2 \tag{7}$$

yielding double pole located at $s = -\rho$. The remaining three design parameters are b, c, and ρ, which should be positive.

IV. Inductance-Adaptation Law

The proposed approach to adjust the inductance estimates is to use an adaptation law

$$\hat{L} = \int \boldsymbol{k}_\mathrm{L}\tilde{\boldsymbol{i}}_\mathrm{s}\mathrm{d}t \tag{8}$$

where $\boldsymbol{k}_\mathrm{L}$ is chosen to utilize the estimation error only in the d-axis direction, $\boldsymbol{k}_\mathrm{L} = [k_\mathrm{L}, 0]$, and the adaptation gain k_L should be positive. If k_L is small, then the original dynamics (6) remain approximately intact. The method is closely related to the permanent-magnet flux adaptation law proposed in [15]. The estimate $\hat{L}$ can be the d-axis inductance estimate $\hat{L}_\mathrm{d}$ or the q-axis inductance estimate $\hat{L}_\mathrm{q}$.

A. $\hat{L}_\mathrm{d}$ Is Adapted

If the adaptation law (8) combined with the full-order observer is used to update the d-axis inductance estimate, it can be shown from (1) – (4) and (8) that the equation for the steady-state position error $\tilde{\vartheta}_{\mathrm{m}0}$ is

$$A\cos(2\tilde{\vartheta}_{\mathrm{m}0}) + B\sin(2\tilde{\vartheta}_{\mathrm{m}0}) + C = 0 \tag{9}$$

where

$$A = (L_\mathrm{d} - L_\mathrm{q})\beta \tag{10a}$$
$$B = L_\mathrm{d} - L_\mathrm{q} \tag{10b}$$
$$C = 2\hat{L}_\mathrm{q}\beta - 2\tilde{R}_\mathrm{s}/\hat{\omega}_\mathrm{m} - \beta(L_\mathrm{d} + L_\mathrm{q}) \tag{10c}$$

and $\tilde{R}_\mathrm{s} = \hat{R}_\mathrm{s} - R_\mathrm{s}$ is the resistance-estimation error. It can be seen that the position error increases when the load increases and the rotational speed of the motor decreases, which indicates that the scheme should be used at high speeds and low loads.

The general solution for the steady-state d-axis inductance estimate is

$$\begin{aligned}\hat{L}_\mathrm{d} =& \frac{L_\mathrm{d} - L_\mathrm{q}}{2}\cos(2\tilde{\vartheta}_\mathrm{m0}) - \beta\frac{L_\mathrm{d} - L_\mathrm{q}}{2}\sin(2\tilde{\vartheta}_\mathrm{m0}) \\ &+ \frac{L_\mathrm{d} + L_\mathrm{q}}{2} - \frac{\beta\tilde{R}_\mathrm{s}}{\hat{\omega}_\mathrm{m}}.\end{aligned} \tag{11}$$

Characteristic behaviour of the d-axis inductance estimation error at different loads with 20% parameter uncertainty is depicted in Fig. 1.

B. $\hat{L}_\mathrm{q}$ Is Adapted

If the adaptation law (8) combined with the full-order observer is used to update the q-axis inductance estimate, the position-error equation (9) is still valid, but the coefficients in this case are

$$A = L_\mathrm{d} - L_\mathrm{q} \tag{12a}$$
$$B = -\beta(L_\mathrm{d} - L_\mathrm{q}) \tag{12b}$$
$$C = (L_\mathrm{d} - 2\hat{L}_\mathrm{d} + L_\mathrm{q}) - \frac{2\tilde{R}_\mathrm{s}\beta}{\hat{\omega}_\mathrm{m}} \tag{12c}$$

It can be seen that in this case the position error decreases when the load and the rotational speed of the motor increase. The general solution for the steady-state q-axis inductance estimate is

$$\begin{aligned}\hat{L}_\mathrm{q} =& \frac{L_\mathrm{d} + L_\mathrm{q}}{2} - \frac{L_\mathrm{d} - L_\mathrm{q}}{2}\cos(2\tilde{\vartheta}_\mathrm{m0}) \\ &+ \frac{\tilde{R}_\mathrm{s}}{\beta\hat{\omega}_\mathrm{m}} - \frac{L_\mathrm{d} - L_\mathrm{q}}{2\beta}\sin(2\tilde{\vartheta}_\mathrm{m0})\end{aligned} \tag{13}$$

Characteristic behaviour of the q-axis inductance estimation error at different loads with 20% parameter uncertainty is depicted in Fig. 2.

V. Stator-Resistance Adaptation Law

A. High-Frequency Signal Injection

A high-frequency voltage excitation is superimposed on the stator voltage in the estimated d-axis direction [19],

$$\boldsymbol{u}_\mathrm{c} = \begin{bmatrix} u_\mathrm{c}\cos(\omega_\mathrm{c}t) \\ 0 \end{bmatrix}. \tag{14}$$

where u_c and ω_c are the magnitude and the frequency of the injected voltage, respectively. The high-frequency current responses depend on the position error,

$$i_\mathrm{dc} = \frac{u_\mathrm{c}\sin(\omega_\mathrm{c}t)}{\omega_\mathrm{c}L_\mathrm{det}}\Big[L_\Sigma - L_\Delta\cos(2\tilde{\vartheta}_\mathrm{m}) - L_\mathrm{dq}\sin(2\tilde{\vartheta}_\mathrm{m})\Big] \tag{15a}$$
$$i_\mathrm{qc} = \frac{u_\mathrm{c}\sin(\omega_\mathrm{c}t)}{\omega_\mathrm{c}L_\mathrm{det}}\Big[L_\Delta\sin(2\tilde{\vartheta}_\mathrm{m}) - L_\mathrm{dq}\cos(2\tilde{\vartheta}_\mathrm{m})\Big] \tag{15b}$$

where

$$L_\mathrm{det} = L_\mathrm{dd}L_\mathrm{qq} - L_\mathrm{dq}^2 \tag{16a}$$
$$L_\Sigma = \frac{L_\mathrm{dd} + L_\mathrm{qq}}{2} \tag{16b}$$
$$L_\Delta = \frac{L_\mathrm{dd} - L_\mathrm{qq}}{2} \tag{16c}$$

and

$$L_\mathrm{dd} = \frac{\partial\psi_\mathrm{d}}{\partial i_\mathrm{d}}, \quad L_\mathrm{dq} = \frac{\partial\psi_\mathrm{d}}{\partial i_\mathrm{q}}, \quad L_\mathrm{qq} = \frac{\partial\psi_\mathrm{q}}{\partial i_\mathrm{q}}. \tag{16d}$$

The method proposed in [20] is to use a combination of the d- and q-axis current components in the position estimation, which is then demodulated and low-pass filtered (LPF) [18], [21],

$$\begin{aligned}\epsilon &= \mathrm{LPF}\left\{\left(\frac{\hat{L}_\mathrm{dq}}{\hat{L}_\mathrm{qq}}i_\mathrm{d} + i_\mathrm{q}\right)\sin(\omega_\mathrm{c}t)\right\} \\ &\approx \frac{\alpha_\mathrm{i}}{s + \alpha_\mathrm{i}}k_\epsilon\sin(2\tilde{\vartheta}_\mathrm{m})\end{aligned} \tag{17}$$

where $\hat{L}_\mathrm{dq}$ is the estimated incremental inductance between the two axis, $\hat{L}_\mathrm{qq}$ is the estimated q-axis incremental inductance, α_i is the bandwidth of the low-pass filter, and k_ϵ is the signal-injection gain given by

$$k_\epsilon = \frac{u_\mathrm{c}}{\omega_\mathrm{c}}\frac{L_\Delta L_\mathrm{qq} - L_\mathrm{dq}^2}{2L_\mathrm{det}L_\mathrm{qq}}. \tag{18}$$

The ratio $\hat{L}_\mathrm{dq}/\hat{L}_\mathrm{qq}$ can be regarded as a compensation factor, which can also include model and implementation uncertainties.

B. Proposed Adaptation Mechanism

The stator-resistance adaptation mechanism proposed in this paper is to feed the error signal ϵ obtained from (17) to the PI mechanism

$$\hat{R}_\mathrm{s} = \gamma_\mathrm{p}\epsilon + \int\gamma_\mathrm{i}\epsilon\mathrm{d}t. \tag{19}$$

When the resistance-adaptation mechanism is combined with the full-order observer, and it is assumed that in the steady state $\tilde{\vartheta}_\mathrm{m0} = 0$, it can be shown from (1) – (4) that the steady-state resistance-estimation error is

$$\tilde{R}_\mathrm{s} = \hat{\omega}_\mathrm{m}\frac{\tilde{L}_\mathrm{d}k_1 + \tilde{L}_\mathrm{q}\beta(k_2 - \hat{\omega}_\mathrm{m})}{k_2 - \hat{\omega}_\mathrm{m} - \beta k_1} \tag{20}$$

where $\tilde{L}_\mathrm{d} = \hat{L}_\mathrm{d} - L_\mathrm{d}$ and $\tilde{L}_\mathrm{q} = \hat{L}_\mathrm{q} - L_\mathrm{q}$.

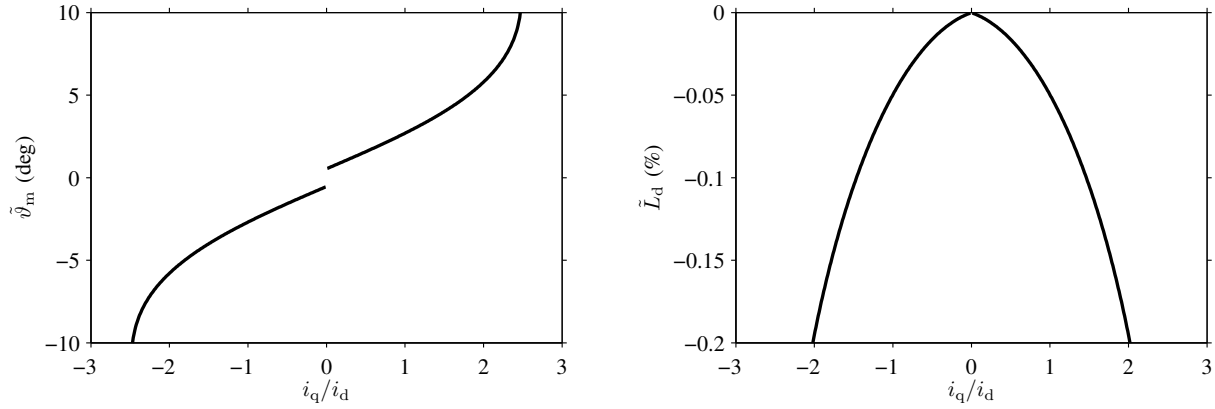

(a) (b)

Fig. 1. Characteristic behaviour of the d-axis inductance adaptation at different loads with 20% parameter uncertainty: (a) position estimation error, (b) inductance estimation error. The q-axis inductance is $L_\mathrm{q} = 0.3$ p.u., the stator resistance is $R_\mathrm{s} = 0.04$ p.u., and the speed is $\hat{\omega}_\mathrm{m} = 0.5$ p.u.

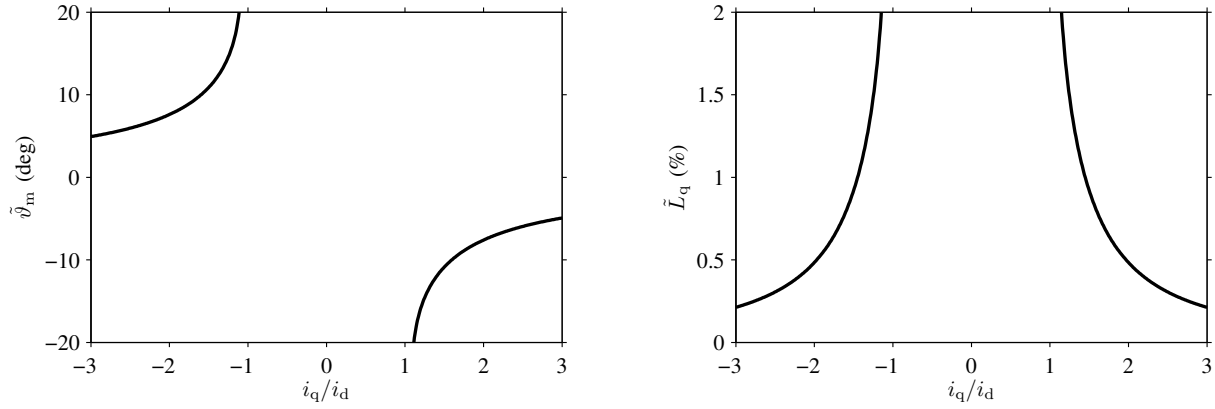

(a) (b)

Fig. 2. Characteristic behaviour of the q-axis inductance adaptation at different loads with 20% parameter uncertainty: (a) position estimation error, (b) inductance estimation error. The d-axis inductance is $L_\mathrm{d} = 2.0$ p.u., the stator resistance is $R_\mathrm{s} = 0.04$ p.u., and the speed is $\hat{\omega}_\mathrm{m} = 1$ p.u.

C. Proposed Gain Selection

The stator-resistance adaptation (19) affects the dynamics of the closed-loops system, and the tuning of the augmented observer has to be reconsidered. The gain selection (3b) is lifted, and alternative formulation for k_1 and k_2 has to be used, when the stator-resistance adaptation is active.

It is assumed that the speed-tracking loop (4) is faster than the resistance-adaptation loop and the flux observer. The characteristic polynomial of the linearized closed-loop system consisting of (1), (2), (3) and (17) – (19) is

$$s^4 + A_1 s^3 + A_2 s^2 + A_3 s + A_4 \tag{21a}$$

where

$$A_1 = \alpha_\mathrm{i} - k_1 + \beta k_2 \tag{21b}$$

$$A_2 = \frac{2k_\epsilon}{L_\mathrm{d} - L_\mathrm{q}} \alpha_\mathrm{i} \beta \gamma_\mathrm{p} - \alpha_\mathrm{i}(k_1 - \beta k_2) - \hat{\omega}_\mathrm{m}(k_2 - \hat{\omega}_\mathrm{m} + \beta k_1) \tag{21c}$$

$$A_3 = \frac{2k_\epsilon}{L_\mathrm{d} - L_\mathrm{q}} \alpha_\mathrm{i} \left[\beta\gamma_\mathrm{i} + \gamma_\mathrm{p}(k_2 - \hat{\omega}_\mathrm{m} - \beta k_1)\right] - \alpha_\mathrm{i}\hat{\omega}_\mathrm{m}(k_2 - \hat{\omega}_\mathrm{m} + \beta k_1) \tag{21d}$$

$$A_4 = \frac{2k_\epsilon}{L_\mathrm{d} - L_\mathrm{q}} \alpha_\mathrm{i}\gamma_\mathrm{i}(k_2 - \hat{\omega}_\mathrm{m} - \beta k_1) \tag{21e}$$

For design purposes, the characteristic polynomial is written in the form

$$(s^2 + Bs + C)(s + \alpha_1)(s + \alpha_2). \tag{22}$$

Equating (21) and (22), the gains of the augmented observer can be written as functions of the design parameters

$\{B, C, \alpha_1, \alpha_2\}$, which all should be positive in order to stabilize the system.

In general case, equating (21) and (22) leads to quadratic or cubic equations, depending on the set of variables to be solved. If the bandwidth of the low-pass filter in (17) is chosen so that $\alpha_\mathrm{i} \gg \{\alpha_2, (-B+\sqrt{B^2-4C})/2, (-B-\sqrt{B^2-4C})/2\}$, then $\alpha_1 \approx \alpha_\mathrm{i}$ and the gains can be approximated as

$$k_1 = \beta k_2 - \alpha_2 - B \tag{23a}$$

$$\gamma_\mathrm{i} = \frac{C\alpha_2}{A(k_2 - \hat{\omega}_\mathrm{m} - \beta k_1)} \tag{23b}$$

$$\gamma_\mathrm{p} = \frac{C + B\alpha_2 + \hat{\omega}_\mathrm{m}(k_2 - \hat{\omega}_\mathrm{m} + \beta k_1)}{A(k_2 - \hat{\omega}_\mathrm{m} - \beta k_1)} + \frac{C\alpha_2 - A\alpha_\mathrm{i}\beta\gamma_\mathrm{i}}{A\alpha_\mathrm{i}(k_2 - \hat{\omega}_\mathrm{m} - \beta k_1)} \tag{23c}$$

where k_2 is a free variable and

$$A = \frac{2k_\epsilon}{L_\mathrm{d} - L_\mathrm{q}}. \tag{24}$$

If k_2 is selected according to (3b), then k_1 approaches the definition used in (3b) when $\alpha_2 \to 0$, $B \to b$, and $C \to c$.

It might happen so that the denominator $k_2 - \hat{\omega}_\mathrm{m} - \beta k_1$ in (23) becomes small, which makes the gains γ_p and γ_i large, and increases sensitivity to load transients and noise. In order to reduce this sensitivity, γ_i can be chosen as a free variable, and $\{\gamma_\mathrm{p}, k_1, k_2\}$ are solved as functions of $\{\gamma_\mathrm{i}, \alpha_2, B, C\}$,

$$k_1 = \frac{B + \alpha_2 - \beta\hat{\omega}_\mathrm{m}}{\beta^2 - 1} - \frac{C\alpha_2\beta}{A\gamma_\mathrm{i}(\beta^2 - 1)} \tag{25a}$$

$$k_2 = \frac{\beta(B + \alpha_2) - \hat{\omega}_\mathrm{m}}{\beta^2 - 1} - \frac{C\alpha_2}{A\gamma_\mathrm{i}(\beta^2 - 1)} \tag{25b}$$

$$\gamma_\mathrm{p} = \frac{C + B\alpha_2 + \hat{\omega}_\mathrm{m}(k_2 - \hat{\omega}_\mathrm{m} + \beta k_1)}{A(k_2 - \hat{\omega}_\mathrm{m} - \beta k_1)} + \frac{C\alpha_2 - A\alpha_\mathrm{i}\beta\gamma_\mathrm{i}}{A\alpha_\mathrm{i}(k_2 - \hat{\omega}_\mathrm{m} - \beta k_1)} \tag{25c}$$

This gain selection should be used only when $\beta^2 \lesssim 0.5$ in order to prevent the denominator $\beta^2 - 1$ becoming close to zero.

VI. Experimental Setup and Implementation

The motion-sensorless control system was implemented in a dSPACE DS1104 PPC/DSP board. A 6.7-kW four-pole SyRM was fed by a frequency converter that is controlled by the DS1104 board. The rated values of the SyRM are: speed 3175 r/min; frequency 105.8 Hz; line-to-line rms voltage 370 V; rms current 15.5 A; and torque 20.1 Nm. The base values for angular speed, voltage, and current are defined as $2\pi \cdot 105.8$ rad/s, $\sqrt{2/3} \cdot 370$ V, and $\sqrt{2} \cdot 15.5$ A, respectively.

A servo motor was used as a loading machine. The rotor speed ω_m and position ϑ_m were measured using an incremental encoder for monitoring purposes. The total moment of inertia of the experimental setup is 0.015 kgm^2 (2.7 times the inertia of the SyRM rotor).

The stator currents and the DC-link voltage were measured, and the reference voltage obtained from the current controller was used for the observer. The sampling was synchronized to the modulation, and both the switching frequency and the sampling frequency were 5 kHz. A simple current feedforward compensation for dead times and power device voltage drops was applied.

TABLE I
Per-Unit Parameters for Saturation Model

L_du	L_qu	α	γ	δ	a	b	c	d
2.73	0.843	0.333	5.58	2.60	6.6	0.8	1	0

The control system was augmented with a speed controller, whose feedback signal was the speed estimate $\hat{\omega}_\mathrm{m}$ obtained from the observer. The bandwidth of this PI controller, including active damping [22], was 0.03 p.u. The estimated stator resistance used in inductance adaptation is $\hat{R}_\mathrm{s} = 0.042$ p.u. and the magnetic saturation has been modeled as functions of the estimated flux [23],

$$i_\mathrm{d} = \frac{\psi_\mathrm{d}}{L_\mathrm{du}}\left(1 + \alpha|\psi_\mathrm{d}|^a + \frac{\delta L_\mathrm{du}}{d+2}|\psi_\mathrm{d}|^c|\psi_\mathrm{q}|^{d+2}\right) \tag{26a}$$

$$i_\mathrm{q} = \frac{\psi_\mathrm{q}}{L_\mathrm{qu}}\left(1 + \gamma|\psi_\mathrm{q}|^b + \frac{\delta L_\mathrm{qu}}{c+2}|\psi_\mathrm{d}|^{c+2}|\psi_\mathrm{q}|^d\right) \tag{26b}$$

where all parameters should be positive. The saturation model parameters are given in Table I.

A smooth transition from standstill to high-speed operation is implemented by decreasing the injected voltage as the speed increases,

$$u_\mathrm{c} = u_\mathrm{c0} f(\hat{\omega}_\mathrm{m}) \tag{27}$$

where the transition function is

$$f(\hat{\omega}_\mathrm{m}) = \begin{cases} 1 - \left|\frac{\hat{\omega}_\mathrm{m}}{\omega_\Delta}\right|, & \text{if } |\hat{\omega}_\mathrm{m}| \le \omega_\Delta \\ 0, & \text{otherwise,} \end{cases} \tag{28}$$

and $u_\mathrm{c0} = 0.1$ p.u. and $\omega_\Delta = 0.1$ p.u. Other design parameters values were: $\omega_\mathrm{c} = 2\pi \cdot 500$ rad/s, $\alpha_\mathrm{i} = 0.3$ p.u., $\alpha_2 = 0.02 \cdot f(\hat{\omega}_\mathrm{m})$ p.u., $B = b = 0.2$ p.u., $c = 20 \cdot b\hat{\omega}_\mathrm{m}^2$ p.u., $C = 0.0178 \cdot f(\hat{\omega}_\mathrm{m}) + c[1 - f(\hat{\omega}_\mathrm{m})]$ p.u., $\rho = 2$ p.u., and $\hat{L}_\mathrm{dq}/\hat{L}_\mathrm{qq} = -0.4 \cdot \mathrm{sgn}(i_\mathrm{q})$. The gain selection was based on (23) and k_2 was selected according to (3b). The resistance estimate seen by other system, such as the current controller, is obtained using a 0.5-Hz low-pass filter for the internal resistance estimate of the flux observer.

VII. Simulation and Experimental Results

Simulation results of the inductance-adaptation law in no load are depicted in Fig. 3(a). The speed reference is $\hat{\omega}_\mathrm{m} = 0.5$ p.u. and the d-axis current reference is 0.5 p.u. The adaptation is turned on at $t = 2$ s with adaptation gain $k_\mathrm{L} = 0.01$ p.u. and initial value $\hat{L}_\mathrm{d} = 2.2$ p.u. It can be seen that the estimated inductance converges to the actual value (2.0 p.u.) in the timescale of the adaptation gain (≈ 0.5 Hz), and the position error decreases simultaneously.

Similar results for the experimental setup are depicted in Fig. 3(b). Since the actual machine saturates, the initial value of the actual inductance is slightly smaller than the final value

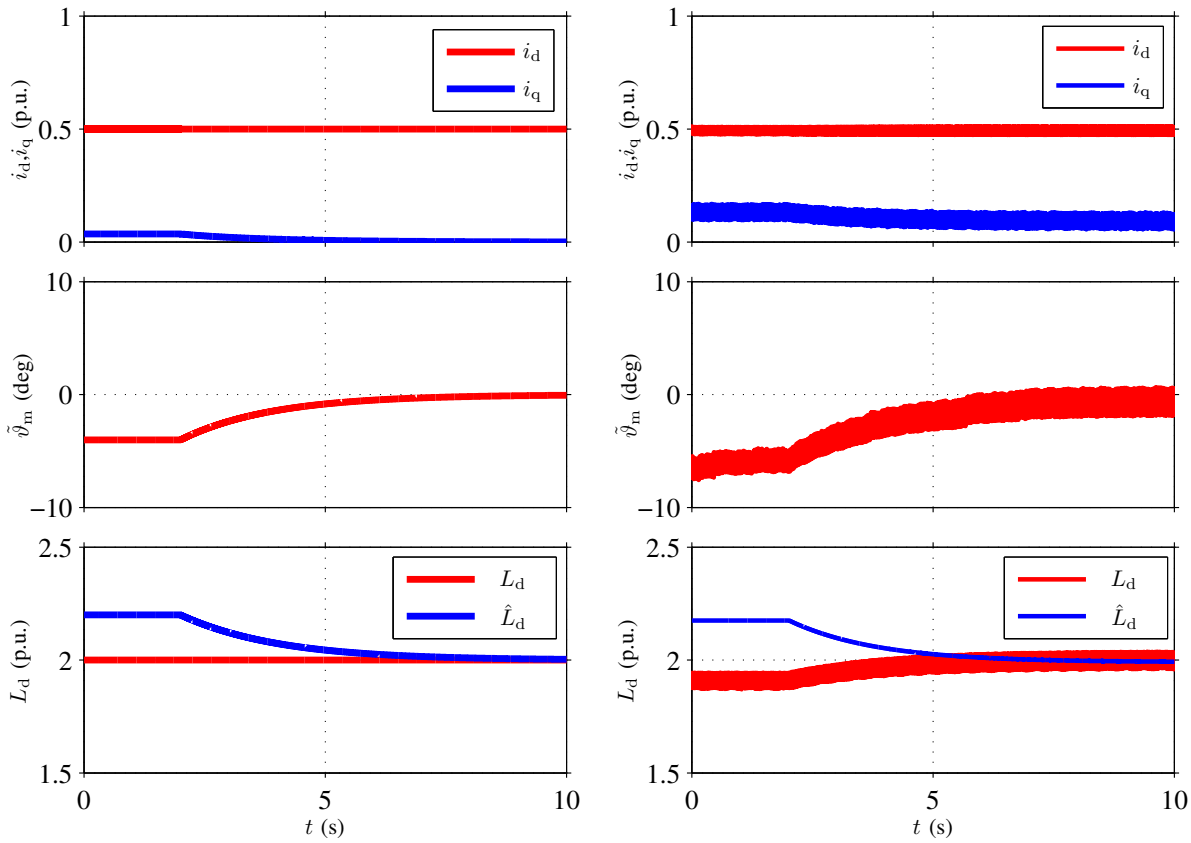

Fig. 3. Results of the inductance adaptation in no load: (a) simulated case, (b) experimental case. The d-axis current is $i_\mathrm{d} = 0.5$ p.u., and the speed reference is $\hat{\omega}_\mathrm{m} = 0.5$ p.u. The adaptation is turned on at $t = 2$ s.

due to position error. The final value of the estimated inductance coincides with the mean value of the actual inductance, and the mean value of the position error is close to zero. In this experiment, the bandwidth of the adaptation is chosen small in order to prevent the inductance estimate from following the inductance harmonics. The method is intended to be used in an initialization test in a fashion similar to [14], after which the saturation-model parameters can be locked.

Experimental results of load-torque steps when the speed reference was kept at 0 are shown in Fig. 4(a). Initially, the negative rated load torque was applied. The load torque was reversed at $t = 5.0$ s and reversed again at $t = 7.5$ s. It can be seen that the filtered resistance estimate in the third subplot recovers rapidly from a sudden load reversal, and the variation is nearly independent of the sign of the load, as predicted by the analysis. The small variation originates from the fact that in the analysis it was assumed that the steady-state position error is zero, which is not actually the case.

Experimental results of a sloped speed reversal from $\hat{\omega}_\mathrm{m} = 0.05$ p.u. to $\hat{\omega}_\mathrm{m} = -0.05$ p.u. and then back to $\hat{\omega}_\mathrm{m} = 0.05$ p.u. with the negative rated load torque applied are shown in Fig. 4(b). The filtered resistance estimate in the third subplot varies with the speed, but the variation remains small. The noise in the estimates originates from saturation-induces saliencies (second harmonic), which is seen as a speed deviation by the speed controller and thus amplified. The noise disappears, as the speed approaches zero.

The actual behaviour of the resistance estimate (19) in Fig. 4(b), when the speed is $\hat{\omega}_\mathrm{m} \approx -0.05$ p.u., is shown in Fig. 5. The solid line is the actual resistance estimate, and the dashed line is the filtered estimate seen by other system, such as the current controller. It can be seen that the resistance estimate varies with twice the rotational frequency. Hence, the resistance estimate (19) should be considered as an internal compensation variable and the filtered resistance estimate as the actual resistance. The resistance estimate in Fig. 4(a) is also low-pass filtered, but since the speed is zero, the harmonic content of the estimate is much smaller than in Fig. 5.

VIII. Conclusions

In this paper, an adaptive full-order observer is augmented with parameter-adaptation laws for SyRM drives. The inductances are adapted using a back-EMF-based method, and the stator resistance is adapted using a signal-injection based method. The analysis and experimental results indicate that the stator-resistance adaptation should be enabled only at low speeds, the d-axis inductance adaptation should be enabled

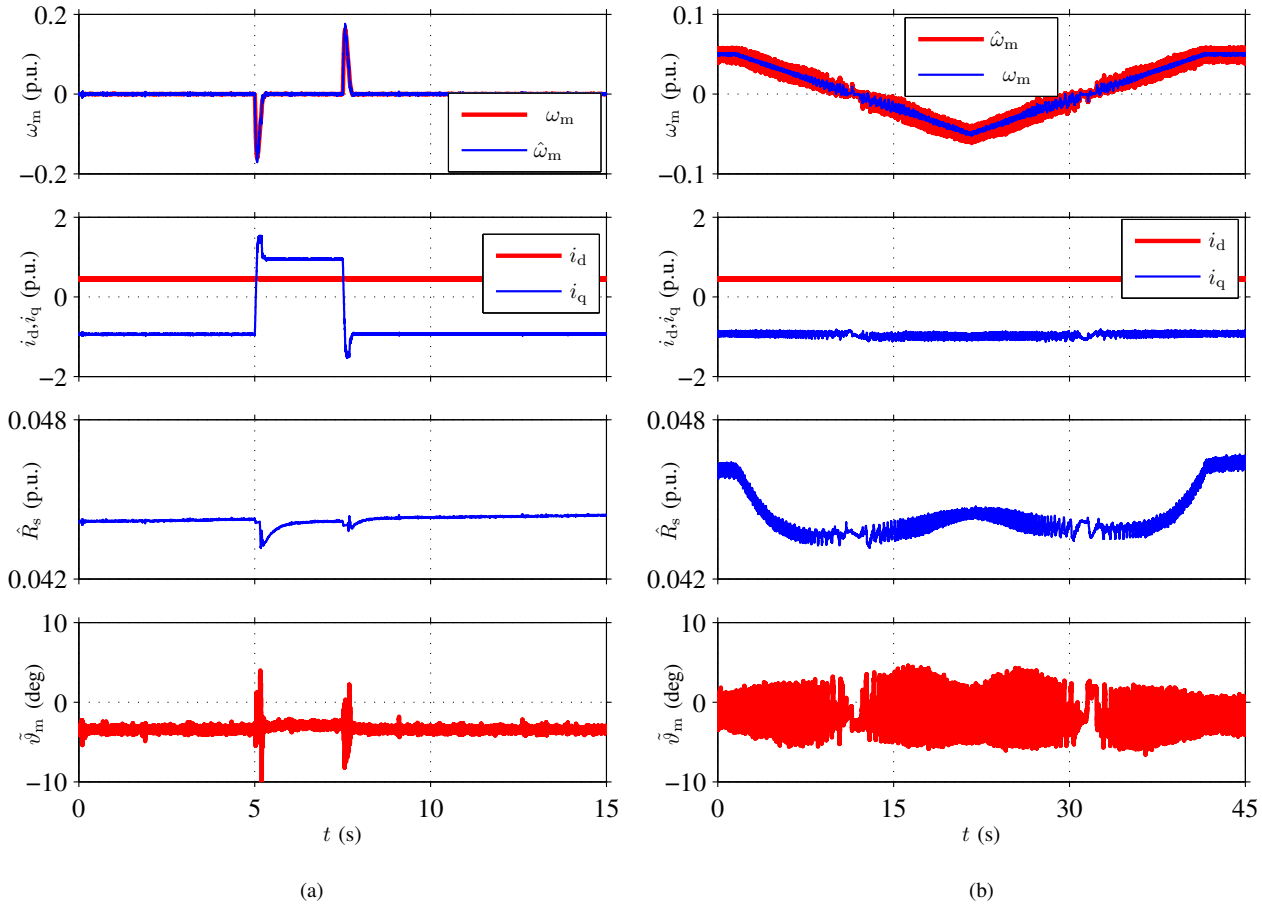

Fig. 4. Experimental results of the stator-resistance estimation: (a) load-torque steps (negative rated → rated → negative rated) when the speed reference is kept at 0; (b) a sloped speed reversal (0.05 p.u. → −0.05 p.u. → 0.05 p.u.) with negative rated load torque applied. The d-axis current is $i_\mathrm{d} = 0.45$ p.u. in both experiments.

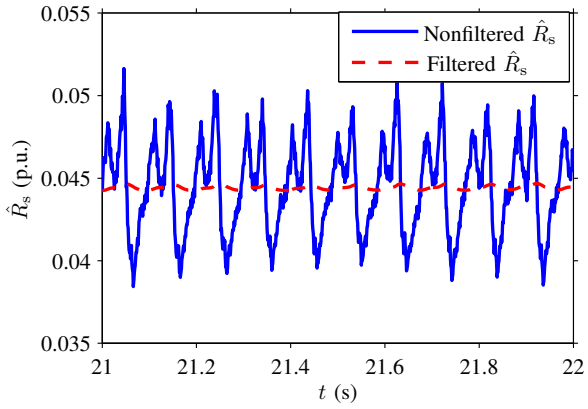

Fig. 5. Behaviour of the resistance estimate, when the estimated speed is −0.05 p.u. in Fig. 4(b). The solid line is the actual estimate and the dashed line is the filtered estimate.

only at medium and high speeds near no load, and the q-axis inductance adaptation should be enabled only at high speeds under high loads. The evaluated schemes demonstrate good performance and both small position error and small parameter estimation errors in laboratory experiments.

ACKNOWLEDGMENT

The authors gratefully acknowledge ABB Oy for the financial support.

REFERENCES

[1] E. Capecchi, P. Guglielmo, M. Pastorelli, and A. Vagati, "Position-sensorless control of the transverse-laminated synchronous reluctance motor," *IEEE Trans. Ind. Appl.*, vol. 37, no. 6, pp. 1768–1776, Nov./Dec. 2001.

[2] H. F. Hofmann, S. R. Sanders, and A. EL-Antably, "Stator-flux-oriented vector control of synchronous reluctance machines with maximized efficiency," *IEEE Trans. Ind. Electron.*, vol. 51, no. 5, pp. 1066–1072, Oct. 2004.

[3] S.-C. Agarlită, I. Boldea, and F. Blaabjerg, "High-frequency-injection-assisted "active flux"-based sensorless vector control of reluctance synchronous motors, with experiments from zero speed," *IEEE Trans. Ind. Appl.*, vol. 48, no. 6, pp. 1931–1939, Nov./Dec. 2012.

[4] J.-I. Ha, S.-J. Kang, and S.-K. Sul, "Position-controlled synchronous reluctance motor without rotational transducer," *IEEE Trans. Ind. Appl.*, vol. 35, no. 6, pp. 1393–1398, Nov./Dec. 1999.

[5] A. Consoli, F. Russo, G. Scarcella, and A. Testa, "Low- and zero-speed sensorless control of synchronous reluctance motors," *Electr. Power Comp. Syst.*, vol. 35, no. 5, pp. 1050–1057, Sep./Oct. 1999.

[6] H. W. de Kock, M. J. Kamper, O. C. Ferreira, and R. M. Kennel, "Position sensorless control of the reluctance synchronous machine considering high frequency inductances," in *Proc. PEDS 2007*, Bangkok, Thailand, Nov. 2007, pp. 812–821.

[7] M. Schroedl and P. Weinmeier, "Sensorless control of reluctance machines at arbitrary operating conditions including standstill," *IEEE Trans. Power Electron.*, vol. 9, no. 2, pp. 225–231, Mar. 1994.

[8] R. Morales-Caporal and M. Pacas, "Encoderless predictive direct torque control for synchronous reluctance machines at very low and zero speed," *IEEE Trans. Ind. Electron.*, vol. 55, no. 12, pp. 4408–4416, Dec. 2008.

[9] T. Matsuo and T. A. Lipo, "Rotor position detection scheme for synchronous reluctance motor based on current measurements," *IEEE Trans. Ind. Appl.*, vol. 31, no. 4, pp. 860–868, July/Aug. 1995.

[10] M.-Y. Wei and T.-H. Liu, "A high-performance sensorless position control system of a synchronous reluctance motor using dual current-slope estimating technique," *IEEE Trans. Ind. Electron.*, vol. 59, no. 9, pp. 3411–3426, Sept. 2012.

[11] A. Piippo, M. Hinkkanen, and J. Luomi, "Sensorless control of PMSM drives using a combination of voltage model and HF signal injection," in *Conf. Rec. IEEE-IAS Annu. Meeting*, vol. 2, Seattle, WA, Oct. 2004, pp. 964–970.

[12] O. Wallmark, L. Harnefors, and O. Carlson, "An improved speed and position estimator for salient permanent-magnet synchronous motors," *IEEE Trans. Ind. Electron.*, vol. 52, no. 1, pp. 255–262, Feb. 2005.

[13] W. Hammel and R. M. Kennel, "Position sensorless control of PMSM by synchronous injection and demodulation of alternating carrier voltage," in *Proc. IEEE SLED 2010*, Padova, Italy, July 2010, pp. 56–63.

[14] M. Ranta and M. Hinkkanen, "Online identification of parameters defining the saturation characteristics of induction machines," in *Proc. ICEM'12*, Marseille, France, Sept. 2012, pp. 1027–1033.

[15] A. Piippo, M. Hinkkanen, and J. Luomi, "Adaptation of motor parameters in sensorless PMSM drives," *IEEE Trans. Ind. Appl.*, vol. 45, no. 1, pp. 203–212, Jan./Feb. 2009.

[16] G. Yang, R. Tomioka, M. Nakano, and T. H. Chin, "Position and speed sensorless control of brushless DC motor based on an adaptive observer," *IEEJ Trans. Ind. Appl.*, vol. 113, pp. 579–586, May 1993.

[17] T. Tuovinen, M. Hinkkanen, L. Harnefors, and J. Luomi, "Comparison of a reduced-order observer and a full-order observer for sensorless synchronous motor drives," *IEEE Trans. Ind. Appl.*, vol. 48, no. 6, pp. 1959–1967, Nov./Dec. 2012.

[18] L. Harnefors and H.-P. Nee, "A general algorithm for speed and position estimation of AC motors," *IEEE Trans. Ind. Electron.*, vol. 47, no. 1, pp. 77–83, Feb. 2000.

[19] M. J. Corley and R. D. Lorenz, "Rotor position and velocity estimation for a salient-pole permanent magnet synchronous machine at standstill and high speeds," *IEEE Trans. Ind. Appl.*, vol. 34, no. 4, pp. 784–789, Jul./Aug. 1998.

[20] T. Tuovinen and M. Hinkkanen, "Adaptive full-order observer with high-frequency signal injection for synchronous reluctance motor drives," vol. 1, Chicago, IL, May 2013, pp. 683–689.

[21] W. T. Villet, M. J. Kamper, P. Landsmann, and R. Kennel, "Evaluation of a simplified high frequency injection position sensorless control method for reluctance synchronous machine drives," in *Proc. IET PEMD 2012*, vol. 1, Bristol, UK, Mar. 2012, pp. 1–6.

[22] L. Harnefors, "Design and analysis of general rotor-flux-oriented vector control systems," *IEEE Trans. Ind. Electron.*, vol. 48, no. 2, pp. 383–390, Apr. 2001.

[23] Z. Qu, T. Tuovinen, and M. Hinkkanen, "Inclusion of magnetic saturation in dynamic models of synchronous reluctance motors," in *Proc. ICEM'12*, Marseille, France, Sept. 2012, pp. 994–1000.